



Probing supramolecular protein assembly using covalently attached fluorescent molecular rotors

Markéta Kubánková^a, Ismael López-Duarte^a, James A. Bull^a, Devkee M. Vadukul^b, Louise C. Serpell^b, Marie de Saint Victor^c, Eleanor Stride^c, Marina K. Kuimova^{a,*}

^a Chemistry Department, Imperial College London, Exhibition Road, London, SW7 2AZ, UK

^b School of Life Sciences, University of Sussex, Brighton, BN1 9QG, UK

^c Institute of Biomedical Engineering, University of Oxford, Oxford, OX3 7DQ, UK

ARTICLE INFO

Article history:

Received 16 February 2017

Received in revised form

22 May 2017

Accepted 5 June 2017

Available online 7 June 2017

Keywords:

Amyloid aggregation

Microviscosity

Fluorescence lifetime imaging microscopy

(FLIM)

Sensors for Aβ(1–42) aggregates

Live cells

ABSTRACT

Changes in microscopic viscosity and macromolecular crowding accompany the transition of proteins from their monomeric forms into highly organised fibrillar states. Previously, we have demonstrated that viscosity sensitive fluorophores termed ‘molecular rotors’, when freely mixed with monomers of interest, are able to report on changes in microrheology accompanying amyloid formation, and measured an increase in rigidity of approximately three orders of magnitude during aggregation of lysozyme and insulin. Here we extend this strategy by covalently attaching molecular rotors to several proteins capable of assembly into fibrils, namely lysozyme, fibrinogen and amyloid-β peptide (Aβ(1–42)). We demonstrate that upon covalent attachment the molecular rotors can successfully probe supramolecular assembly *in vitro*. Importantly, our new strategy has wider applications *in cellulo* and *in vivo*, since covalently attached molecular rotors can be successfully delivered *in situ* and will colocalise with the aggregating protein, for example inside live cells. This important advantage allowed us to follow the microscopic viscosity changes accompanying blood clotting and during Aβ(1–42) aggregation in live SH-SY5Y cells. Our results demonstrate that covalently attached molecular rotors are a widely applicable tool to study supramolecular protein assembly and can reveal microrheological features of aggregating protein systems both *in vitro* and *in cellulo* not observable through classical fluorescent probes operating in light switch mode.

© 2017 The Authors. Published by Elsevier Ltd. This is an open access article under the CC BY license (<http://creativecommons.org/licenses/by/4.0/>).

1. Introduction

Supramolecular assemblies of proteins in the form of fibrous structures are investigated due to their functional roles in organisms, such as in the case of tubulin, actin and fibrinogen [1]. Protein assemblies called amyloids contain fibrils with β-sheets rich in intermolecular hydrogen bonds, and are associated with a range of neurodegenerative disorders such as Alzheimer's and Parkinson's disease [2].

Due to the unusual properties of amyloid materials, which are of interest to materials sciences [3], as well as in biology and medicine, particularly through their connection with pathological conditions [2], a range of experimental methods has been developed to probe protein aggregation from the soluble monomeric protein

form into amyloid [4–12]. In particular, the change in the fluorescence intensity of small synthetic fluorophores upon binding to amyloid fibrils has been successful in detecting amyloid formation. One of the most popular probes, Thioflavin T (ThT), shows a marked increase in the fluorescence quantum yield upon binding to amyloid fibrils and is often used to probe the dynamics of fibril formation in solution [13]. Likewise, similar ‘light switch’ molecules such as ruthenium(II) dipyrrophenazine complexes [14,15] and others [16–18] have been used successfully to identify amyloid fibril formation *in vitro*.

Recently, our laboratory [19] and other researchers [20] reported that the fluorescence lifetime of viscosity sensitive fluorophores termed ‘molecular rotors’ [21–24] was able to provide additional information about the aggregation of lysozyme and insulin and as such offered significant advantages over traditionally used fluorescence intensity measurements.

In our recent work [19] we used Fluorescence Lifetime Imaging

* Corresponding author.

E-mail address: m.kuimova@imperial.ac.uk (M.K. Kuimova).

(FLIM) of a molecular rotor DiSC₂(3) (Fig. S1a, Supplementary Material) to report on the increasing rigidity during the aggregation of insulin and lysozyme. The use of fluorescence lifetime offered significant benefits compared to the intensity-based measurements. For example, using phasor analysis of time resolved fluorescence decays we were able to report on multiple mechanistic stages of the aggregation process that were unknown previously.

One of the major disadvantages of currently used fluorescence aggregation probes is that due to a non-covalent nature of the interaction between the dye and the protein, these studies are restricted to aggregation reactions carried out *in vitro* and preclude the investigations of aggregation of amyloidogenic proteins in systems where the prior mixing of the rotor and the protein is not feasible, such as in live cells. At the same time it is essential to study such processes in living cells, especially in order to understand the connection between the aggregation, cytotoxicity and *in vivo* pathology of neurodegeneration. It is expected that the mechanism of the process might be affected by the properties of the immediate environment where an aggregation takes place and by the interactions of aggregates with cellular components. Here we report how covalently attaching molecular rotors to a protein of interest can override the disadvantage highlighted above. We demonstrate that fluorescence lifetime of rotors remains a sensitive reporter of the microviscosity and crowding in the immediate environment of the rotor even after covalent attachment to proteins, namely lysozyme, fibrinogen and beta-amyloid. Finally, we use FLIM of covalently bound rotors to follow supramolecular assembly of the proteins of interest *in vitro* and *in cellulo*.

2. Results and discussion

2.1. Viscosity sensitivity of sulfo-Cy3-HEWL conjugates

We first chose a cyanine dye sulfo-Cy3-NHS as a molecular rotor for conjugation (Fig. 1a). Sulfo-Cy3 is a water-soluble dye that is structurally and spectrally similar to DiSC₂(3) (Figs. S1 and S2, Supplementary Material).

Unconjugated DiSC₂(3) was previously used to probe lysozyme and insulin aggregation *via* FLIM and displayed a large dynamic range of lifetimes at different stages of aggregation reaction [19].

We conjugated sulfo-Cy3-NHS to hen egg white lysozyme (HEWL, see Supplementary Material for conjugation conditions),

which represents a well characterised system for probing protein aggregation *in vitro*. Furthermore, self-assembly of lysozyme is associated with systemic amyloidosis [25,26].

As the molecular rotor is small (sulfo-Cy3-NHS $M_r = 735.8$ Da) compared to lysozyme ($M_r = 14307$ Da), and attached *via* a flexible linker, we hypothesised that the sulfo-Cy3-HEWL conjugate would retain its molecular rotor properties and display fluorescence lifetime sensitivity to viscosity.

NHS esters are commonly used for modifying primary amine groups of proteins (Fig. 1c). Aiming to predominantly label the N-terminal amine group of HEWL with sulfo-Cy3-NHS, the conjugation reaction was carried out at pH 6.4. Specifically for HEWL, according to acid base equilibrium at this pH, the N-terminus ($pK_a = 7.9$) is more likely to be available to react with the NHS ester compared to the amine groups on HEWL's five lysine residues (average $pK_a = 10.8$) [27]. We used mass spectrometry to investigate the presence of HEWL monomers labelled with multiple sulfo-Cy3 molecules (Fig. S3, Supplementary Material). From this data it is clear that while a majority of the HEWL monomers were labelled with one sulfo-Cy3, part of HEWL monomers were labelled with two dye molecules, possibly at side-chain amines or at sites other than primary amines [28–30]. While multiple site labelling of HEWL (with one or two dye molecules) is not ideal and can potentially cause more complex time resolved fluorescence decays of a conjugate (see below), it does not preclude accurate data collection of the aggregation process. Importantly, maintaining identical conditions during all conjugation reactions should prevent differences in labelling efficiencies, resulting in comparable fluorescence lifetimes in different reaction runs (Fig. S4, Supplementary Material).

In order to test the viscosity-sensitivity of sulfo-Cy3-HEWL, we measured the time resolved fluorescence decays of the dye in solutions of different viscosities, between 1 and 3628 cP, in sucrose/water mixtures (Fig. 2). The typical set of data (Fig. 2a) recorded in sucrose/water mixtures at a fixed temperature clearly indicates that the fluorescence decay lengthens with increasing viscosity (increasing sucrose percentage), confirming that sulfo-Cy3 retains its properties as a lifetime-based molecular rotor, even when conjugated. Due to a multi-exponential nature of the fluorescence decay we chose to employ phasor analysis [31], a model free representation of the data, to aid the visualisation of the results (Fig. 2b). Phasor analysis of all decays recorded at various sucrose

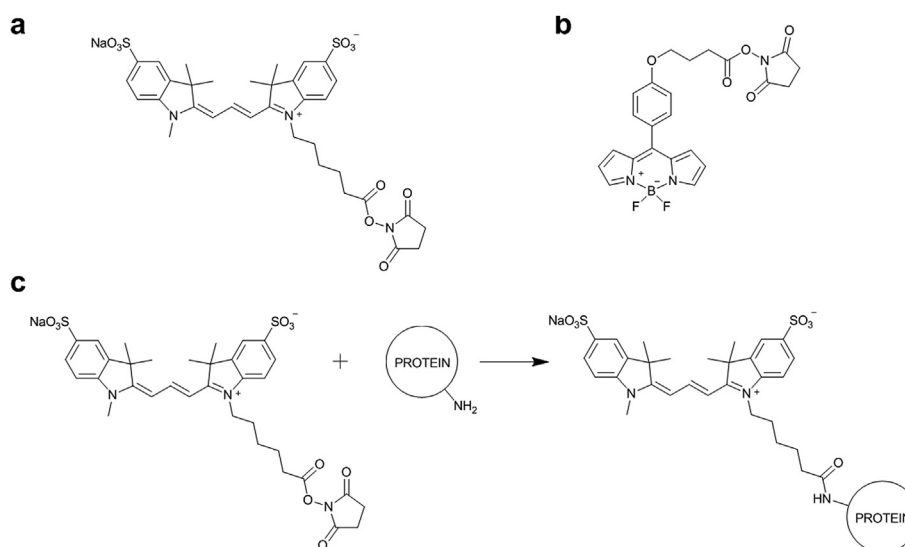


Fig. 1. Molecular structures of (a) sulfo-Cy3-NHS and (b) BODIPY-NHS. (c) A schematic representation of the conjugation reaction.

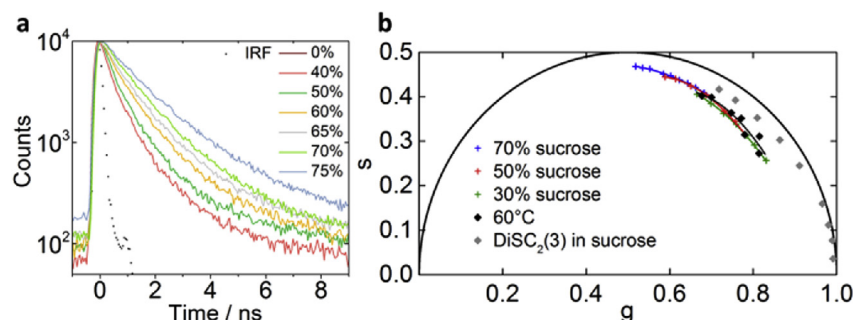


Fig. 2. (a) Fluorescence decays of sulfo-Cy3-HEWL in sucrose solutions of various concentrations at 60 °C, giving the viscosity range 1.2–105 cP; the w/w percentage of sucrose is given in the key. (b) Phasor analysis of the decays shown in (a) (black). Phasors of sulfo-Cy3-HEWL decays recorded at 0 °C to 65 °C are shown in green (30%), red (50%) and blue (70% sucrose solutions). The corresponding viscosity ranges were 1.1–6.7 cP for 30%, 3.8–44.7 cP for 50%, and 39–3628 cP for 70% sucrose solution. The phasors of decays of unconjugated DiSC₂(3) recorded in sucrose solutions of 0.9–190.5 cP are shown in grey. (For interpretation of the references to colour in this figure legend, the reader is referred to the web version of this article.)

concentrations and temperatures demonstrates that in general, the mean fluorescence lifetime of sulfo-Cy3-HEWL increases with increasing viscosity of the sucrose solution (*i.e.* the phasors move from right to left within the universal circle following an increase in viscosity). This again confirms that even after its conjugation to lysozyme, sulfo-Cy3 retains its environment-sensitive photophysics and its fluorescence lifetime should be a useful probe of microscopic viscosity and crowding.

These data could be compared to the calibration set of the structurally similar free dye, DiSC₂(3) (Fig. 2b, grey diamonds). While both sets of data show a large increase in the mean fluorescence lifetime with viscosity, the data for the sulfo-Cy3-HEWL shows a more pronounced deviation from monoexponentiality (*i.e.* the data points on the phasor plot are placed further away from the universal circle). It is likely that the multi-exponential nature of the sulfo-Cy3-HEWL fluorescence decays is caused by dye molecules reporting on several environments due to multiple labelling sites on the protein, which might cause variations in the activation barrier for the intramolecular rotation of sulfo-Cy3. However, data recorded for different batches of labelled protein show close overlap in the phasor space (Fig. S4, Supplementary Material) giving us confidence that the labelling produces photophysically similar rotor-protein constructs.

As could be seen from Fig. 2b, sulfo-Cy3-HEWL displays a considerably higher lifetime (and an anticlockwise-shifted phasor) at 1 cP, compared to DiSC₂(3). This observation is in agreement with previous studies [32,33] which reported an increased isomerisation barrier of cyanine dyes following covalent attachment to DNA. The difference in lifetime between the free dye and a conjugate offered additional control of a conjugation reaction since it meant that we were able to monitor the completion of the reaction by observing the lifetime change of sulfo-Cy3-NHS in the presence of HEWL (Fig. S5, Supplementary Material). All reactions were complete within 6 h of the mixing of the starting components.

It is noteworthy that in these experiments we increased the viscosity of calibration solutions either by (i) increasing sucrose concentration or (ii) by decreasing solution temperature. This allowed us, on one hand, to achieve the widest range of viscosities for calibration and, on the other hand, to test the effect of temperature on the response of our rotor. While the data recorded from various sucrose/water solutions at variable temperature overlap well in the phasor space (Fig. 2b), we detected a slight dependence of the fitted mean lifetime on the temperature of the mixtures (Fig. S6, Supplementary Material). This behaviour indicates that sulfo-Cy3 shows both viscosity- and temperature-dependent lifetimes [34]. Thus, to avoid any contribution of temperature

variations, a calibration set of sulfo-Cy3-HEWL time resolved fluorescence decays was measured in sucrose/water mixtures at 60 °C (Fig. 2a), at the intended temperature of the HEWL aggregation reaction.

2.2. Monitoring lysozyme aggregation using fluorescence lifetime of sulfo-Cy3-HEWL

The aggregation of lysozyme, induced by the combination of heat and low pH, was monitored by recording time-resolved fluorescence decays of sulfo-Cy3-HEWL conjugates (added at 1% to total HEWL) that were measured periodically throughout the reaction until the decays stopped changing and the sample was fully fibrillar (Fig. 3a).

It is clear to see that the mean fluorescence lifetime of sulfo-Cy3-HEWL increased throughout aggregation, which is also evident from observing the counter clockwise trend of the phasors of these decays (Fig. 3b). This corresponds to an increasing restriction of intramolecular rotation of sulfo-Cy3, as the protein undergoes assembly into larger quaternary structures in the vicinity of sulfo-Cy3 and consequently the immediate environment of the rotor becomes more crowded.

Interestingly, the phasor plot of sulfo-Cy3-HEWL during aggregation is a rather simple, monotonic curve, unlike the more complex curve of a free structurally related dye, DiSC₂(3), where a clear change in the phasor trajectory can be observed, indicative of various stages of aggregation (Fig. S7, Supplementary Material) [19]. We hypothesise that the complexity in the case of HEWL aggregation monitored by DiSC₂(3) arises from interactions between the protein units and as such, the covalently bound sulfo-Cy3 may be located at a different site on the protein compared to free DiSC₂(3) and is thus not able to sense the process linked with the non-monotonic trend in the DiSC₂(3) phasor plot.

2.3. Investigation of blood clotting using sulfo-Cy3-fibrinogen

A major advantage of using molecular rotors covalently attached to the protein of interest is the possibility to translate our methodology from cuvette measurements to a true aggregation *in vivo*, where the prior mixing of the components is not possible. To explore this possibility sulfo-Cy3-NHS was conjugated to fibrinogen and used to monitor blood clotting (see Supplementary Material for conjugation conditions).

MALDI and other mass spectrometry instruments available to us were not suitable for studying sulfo-Cy3-fibrinogen conjugates due to a large molecular weight of fibrinogen, thus the fact that sulfo-

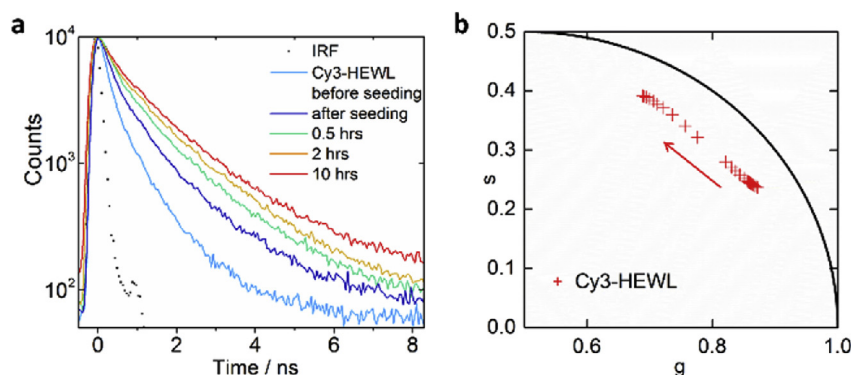


Fig. 3. (a) Fluorescence decays recorded in the course of sulfo-Cy3-HEWL aggregation; (b) Phasor analysis of sulfo-Cy3-HEWL decays during aggregation. Only the centroids of phasor clouds are shown for clarity; the arrow shows the direction of the trend.

Cy3 was covalently linked to fibrinogen was confirmed by the formation of a fluorescent fibrin mesh when blood clotting was induced (Fig. 4a and b, taken before and after clotting, respectively). Furthermore, when the mesh containing sulfo-Cy3-fibrin was disassembled due to the effect of a known clot-dissolving drug, sulfo-Cy3 fluorescence became dimmer and the characteristic mesh structure disappeared, confirming that sulfo-Cy3 and fibrinogen were, in fact, covalently linked (Fig. S8, Supplementary Material).

We first tested the viscosity sensitivity of the sulfo-Cy3-fibrinogen conjugates, Fig. 4c. We recorded time resolved fluorescence decays in solutions of varied viscosities (pure water, pure glycerol, 1:1 water-glycerol mixture) and observed a clear increase in the mean fluorescence lifetime of sulfo-Cy3-fibrinogen (Fig. 4c). Hence, we confirmed again that conjugation does not affect the ability of sulfo-Cy3 to work as a viscosity sensor.

For the blood clotting measurements, sulfo-Cy3-fibrinogen conjugates were added to a sample of blood and fluorescence

signal was collected before and after blood clotting. The presence of a clot was confirmed by confocal microscopy. In Fig. 4a, no organised structure is visible in the blood sample, while in Fig. 4b the fibrin mesh typical for clotted blood is assembled and it is clear that the sulfo-Cy3-fibrin molecules have incorporated into it.

In addition to confocal microscopy, fluorescence decays of sulfo-Cy3-fibrinogen were measured before and after clotting (Fig. 4c). It is clear that the decays recorded after clotting are consistently longer than the decays recorded before clotting, which is consistent with sulfo-Cy3 sensing the crowded environment of the fibrin mesh in the blood clot. While the observed lifetime change was small, it was observable in all repeats of experiments and for different types of clots, e.g. blood, plasma (Fig. S9, Supplementary Material), demonstrating wide applicability of the method. Further rational design should produce a labelling strategy which leads to a more significant change of fluorescence lifetime during blood clotting, which could be practically useful.

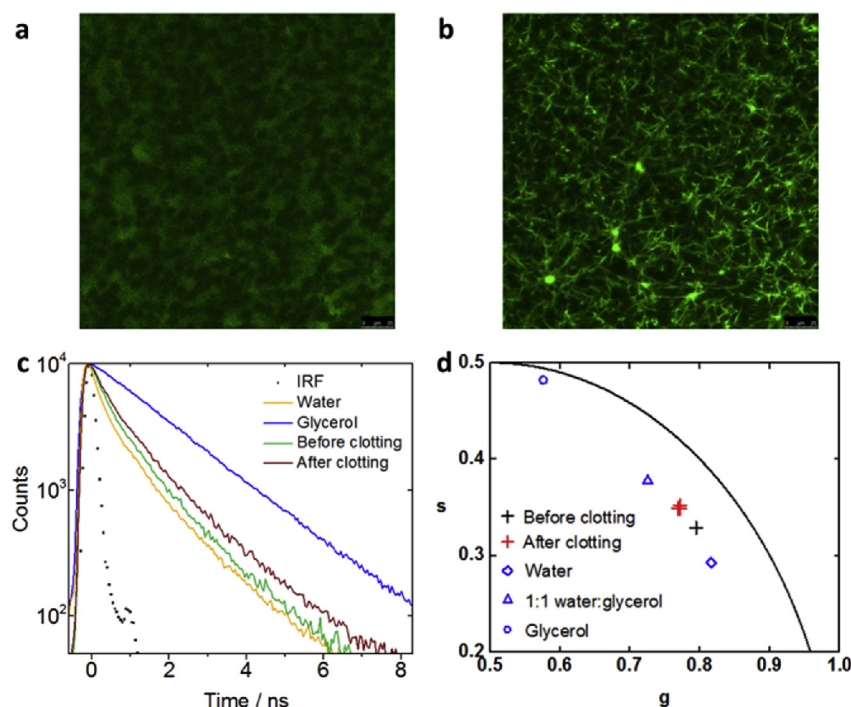


Fig. 4. Confocal images of sulfo-Cy3-fibrin conjugates in human blood recorded before (a) and after (b) clotting; (c) Decays of sulfo-Cy3-fibrin recorded before clotting (green) and after clotting (brown) compared to decays in pure water (orange) and glycerol (blue); (d) Phasors corresponding to decays of sulfo-Cy3-fibrin conjugates in various mixtures as indicated in the key. (For interpretation of the references to colour in this figure legend, the reader is referred to the web version of this article.)

We have compared the microrheological changes observed with molecular rotors during the assembly of various proteins (Fig. S10, Supplementary Material). Clearly, the fluorescence lifetime sensitivity to microviscosity is very dependent on the specific rotor-protein system and is likely to be affected by both the mechanism of aggregation and by the localisation of the rotor. The latter can be specifically engineered if needed and, as such, our strategy represents a powerful tool to study the mechanistic details of supra-molecular protein assembly.

2.4. Monitoring A β (1–42) aggregation using fluorescence lifetime of molecular rotors

We have next tested whether it is possible to monitor protein aggregation with a hydrophobic BODIPY-based molecular rotor, previously used for a range of biological viscosity studies in lipid-based membranes [22,35–42].

BODIPY-C₁₀ (Fig. S1c, Supplementary Material) displays a large dynamic range of lifetimes in the viscosity range between 20 and 5000 cP and is characterised by monoexponential time resolved fluorescence decays in homogeneous media [22,41], and was shown to measure viscosity in temperature-independent manner [34]. However, the use of BODIPY-based rotors in water-based systems was precluded until now due to a poor solubility of the dye in aqueous media.

We have synthesised BODIPY-NHS (Fig. 1b; see Supplementary Material for detailed synthetic procedures and characterisation), covalently linked it to HEWL under conditions similar to sulfo-Cy3-NHS, and used it to monitor HEWL aggregation (see Figs. S11–S13 and the accompanying Supplementary Material text). This data clearly demonstrated that even a hydrophobic molecular rotor can be rendered suitable for probing protein self-assembly in an aqueous media, by covalent conjugation.

Next we set out to study A β (1–42) aggregation in live cells using covalently conjugated BODIPY. Thus we have produced a conjugate of A β (1–42) covalently linked to BODIPY-NHS and added the resulting construct to live SH-SY5Y cells. Without the covalent attachment of the rotor it is not possible to achieve co-localisation of the protein with the viscosity sensor in live cells, since the free-added sensor independently interacts with cells showing efficient endocytosis (Fig. S14, Supplementary Material) [22,41].

We have chosen to monitor the aggregation of A β (1–42) due to its relevance in human disease. The appearance of A β (1–42) aggregates is a hallmark of Alzheimer's disease [2] and the link between A β (1–42) aggregation and the disease onset is still not understood, resulting in great interest in characterising the aggregation process, especially in the more cytotoxic pre-fibrillar stages [43].

A β (1–42) has two lysine residues which, together with the N-terminus, yield three potential labelling sites for BODIPY-NHS. However, our mass spectrometry data provided evidence for the formation of a single-labelled A β (1–42) only (Fig. S15, Supplementary Material). Due to the fact that A β (1–42) starts aggregating immediately after resuspension from film we used a shorter conjugation time of 1 h, compared to the previously described conjugation reactions with HEWL; this shorter conjugation time was possibly responsible for the presence of some unreacted dye in the mixture, as apparent from mass spectrometry (Fig. S15, Supplementary Material).

Transmission electron microscopy (TEM) images were collected to monitor aggregation of A β (1–42) with and without BODIPY labelling (Fig. 5 and Fig. S16, Supplementary Material) to verify that labelling A β (1–42) with BODIPY did not disrupt the secondary structure and aggregation properties of the protein [44]. Additionally, we monitored the kinetics of labelled and unlabelled

A β (1–42) aggregation using the fluorescence intensity of tyrosine [45] (Fig. S17, Supplementary Material). We confirmed that the tyrosine intensity decrease trend is very similar for both unlabelled and BODIPY-labelled A β (1–42) over the course of 48 h. Together, this data confirmed that the morphology of A β (1–42) fibrils and the kinetics of aggregation remained unchanged, in spite of labelling. We also performed a Thioflavin T (ThT) intensity assay [46] of A β (1–42) aggregation to confirm fibril formation at our experimental conditions (Fig. S18, Supplementary Material).

A simple monotonically increasing trend in the rotor lifetime was recorded for BODIPY-A β (1–42) aggregation *in vitro*, Fig. 6i. This increase occurred on a faster timescale compared to a ThT intensity increase (Fig. S18, Supplementary Material), suggesting that, while ThT intensity monitors fibril formation, BODIPY-A β (1–42) lifetime may be sensitive to an earlier stage of aggregation. Previously, a faster kinetics of aggregation was reported during the self-assembly of insulin, when monitored by ThT lifetime as compared to ThT intensity [20].

The consecutive FLIM images of BODIPY-A β (1–42) recorded during the course of the aggregation of A β (1–42) *in cellulo* are shown in Fig. 6a–d along with the corresponding mean lifetime histograms. The evolution of the mean fluorescence lifetime of BODIPY-A β (1–42) *in cellulo* is shown in Fig. 6f. From these data it is clear that the lifetime of BODIPY-A β (1–42) *in cellulo* does not follow a simple monotonically increasing trend recorded for BODIPY-A β (1–42) aggregation at identical conditions *in vitro* (in an identical imaging well with no cells present) (Fig. 6i).

Our cell images (Fig. 6e and Fig. S19, Supplementary Material) suggest that A β (1–42) interacts with cells, in particular with the cellular plasma membrane. The analysis of cell morphology following 4 h of incubation with A β (1–42) aggregates gave evidence for membrane disruption and cell damage, through the rounding up of cells and their detachment from the surface (Fig. S19, Supplementary Material). In addition, it is interesting to note that some of the BODIPY-A β (1–42) aggregates internalised, while some appeared to adhere to SH-SY5Y plasma membranes, which might be due to cells not being able to internalise larger aggregates. We were able to rule out the toxic or disruptive effect of the rotor itself due to the fact that the BODIPY rotors are known to be non-toxic (Fig. S14, Supplementary Material) [47]. Furthermore, BODIPY rotors undergo endocytosis and do not directly interact with cell plasma membranes, unless their chemical structure is specifically altered [22,37,47].

As can be seen from the analysis of mean lifetime evolution throughout the aggregation process (Fig. 6f), the microviscosity sensed by BODIPY-A β (1–42) upon the interaction of A β (1–42) with cells appeared to decrease in the first 2 h from the start of the aggregation, which was followed by a gradual increase resulting in apparent recovery to the initial levels. We note that the timescale of these two phases, decrease and recovery, appears to correspond to two distinct phases of A β (1–42) aggregation monitored by TEM. As could be seen from TEM images (Fig. 6 and Fig. S16, Supplementary Material), in the first 2 h the sample is mostly comprised of monomeric and oligomeric species; however, after ca 3 h the formation of first BODIPY-A β (1–42) fibrils are observed. Thus, it appears that the increase in microviscosity as measured by BODIPY-A β (1–42) in cells coincides with the timescales of formation of the amyloid fibrils. Interestingly, the observed non-monotonic trend does not match the *in vitro* trajectory (see above) and might be due to an interaction with the membrane or due to a different pathway of aggregation itself. For example, the fibril formation may be delayed by the presence of the membrane or the delay in the lifetime increase may reflect the formation of loosely associated A β (1–42) oligomers that later convert into β -strands [43].

The initial mean lifetime of the *in vitro* BODIPY-A β (1–42)

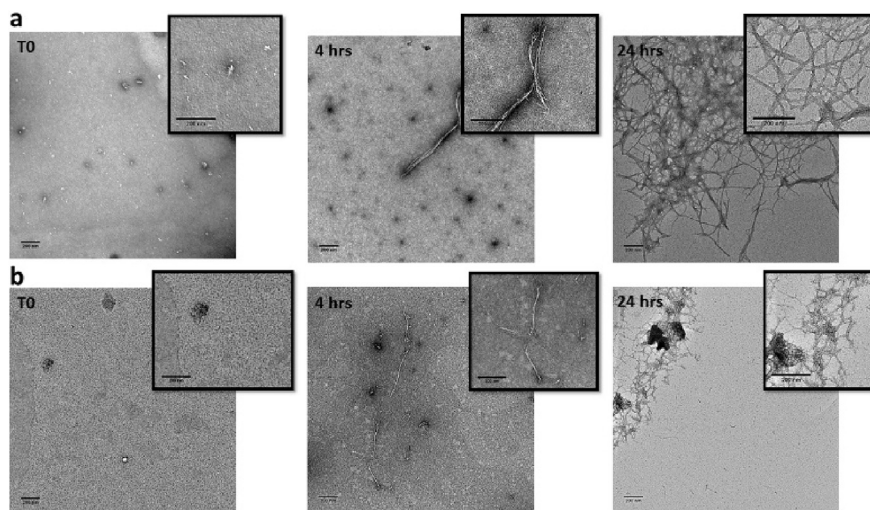


Fig. 5. Transmission electron microscopy (TEM) images of 10 μ M (a) unlabelled A β (1–42) aggregates and (b) BODIPY-A β (1–42) aggregates at times 0, 4 and 24 h after the start of aggregation. Scale bars = 200 nm. Larger versions of the TEM images with more time points are shown in Fig. S16, Supplementary Material.

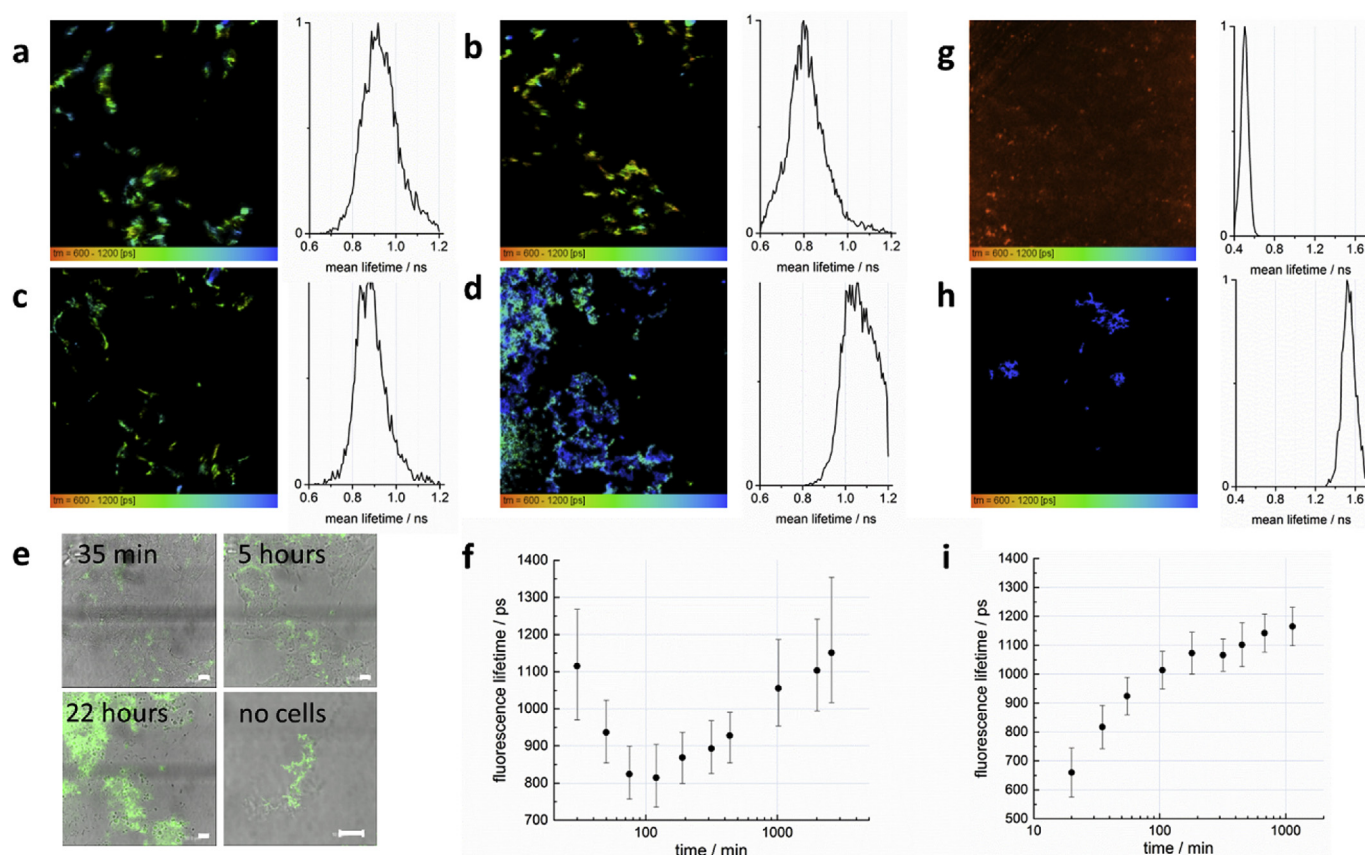


Fig. 6. (a–d) Fluorescence lifetime images of SH-SY5Y cells incubated with BODIPY-A β (1–42) at various time points after the start of the aggregation: 50 min (a), 2 h (b), 7.25 h (c) and 33.5 h (d); (e) Confocal fluorescence overlaid with transmission images of SH-SY5Y cells incubated with BODIPY-A β (1–42) 35 min, 5 h and 22 h after the start of the aggregation; the image of BODIPY-A β (1–42) aggregates after 22 h incubation in a well that did not contain cells is also shown (scale bars = 10 μ m); (f) The evolution of the mean fluorescence lifetime of BODIPY-A β (1–42) during the course of aggregation in the presence of SH-SY5Y cells; (g,h) Fluorescence lifetime images of BODIPY-A β (1–42) in a well that did not contain cells, 10 min (g) and 44 h (h) following sample preparation; (i) The mean fluorescence lifetime of BODIPY-A β (1–42) during the course of aggregation in solution (no cells present), recorded in a separate experimental run, the error bars represent the standard deviation.

mixture was shorter than the first time point *in cellulo* (compare Fig. 6a and g), possibly because the immediate interaction of A β (1–42) with SH-SY5Y plasma membranes either created a more viscous environment for the rotor or changed the peptide structure

itself [48]. A true ‘time 0’ lifetime measurement for purely monomeric A β (1–42) solution could not be obtained either *in cellulo* nor *in vitro*, as A β (1–42) aggregation starts immediately after the resuspension from film and thus may proceed during the

conjugation reaction.

The differences between the fluorescence lifetime trends recorded during the aggregation of BODIPY- $\text{A}\beta(1-42)$ *in vitro* and *in cellulo* are striking and indicate that the mechanistic details of the process are strongly affected by the presence of cellular membranes, as predicted by molecular dynamics simulations [48]. As such, rather than using simplified models, our method allows to follow the mechanism of complex biological processes in their natural environment, such as protein aggregation in live cells, and provides information that was unavailable previously. In the future, we foresee that our rotor-based method can be employed as an assay for investigating new molecules tested as potential inhibitors of aggregation *in vitro* and *in cellulo*, since these inhibitors are an important potential strategy for therapeutic intervention [49–51].

3. Conclusions

We have employed cyanine-based and BODIPY-based viscosity-sensitive fluorescent molecular rotors to monitor the supramolecular assembly of various proteins. The molecular rotors were covalently linked to the aggregating proteins, which provided a unique possibility to monitor the aggregation process *in cellulo*, in addition to *in vitro* studies. Our approach of conjugating the viscosity-sensitive rotor to the protein of interest allowed us to observe increasing molecular crowding during protein aggregation *in vitro* and *in cellulo*. Our findings demonstrate that *in vitro* experiments may not reflect the true behaviour of proteins assembling in their natural biological intra- or extracellular environment, thus emphasising the importance of conducting experiments *in cellulo*. Our results prove that molecular rotors covalently conjugated to proteins of interest provide a unique tool for studying the supramolecular assembly of proteins both *in vitro* and *in cellulo*.

Acknowledgements

MK is thankful for an Imperial College President's PhD Scholarship. MKK is thankful to the EPSRC for the Career Acceleration Fellowship (EP/I003983/1). ES and MdSV also thank the EPSRC for funding under grant EP/I021795/1 and the Research Council UK Digital Economy Programme, through the Centre for Doctoral Training in Healthcare Innovation (EP/G036861/1).

Appendix A. Supplementary data

Supplementary data related to this article can be found at <http://dx.doi.org/10.1016/j.biomaterials.2017.06.009>.

References

- [1] B. Pieters, M. van Eldijk, R. Nolte, J. Mecnović, *Chem. Soc. Rev.* 45 (2016) 24–39.
- [2] D.J. Selkoe, *Nat. Cell Biol.* 6 (2004) 1054–1061.
- [3] T.P.J. Knowles, M.J. Buehler, *Nat. Nanotechnol.* 6 (2011) 469–479.
- [4] M. Staderini, M.A. Martin, M.L. Bolognesi, J.C. Menéndez, *Chem. Soc. Rev.* 44 (2015) 1807–1819.
- [5] C.J. Sigurdson, K.P.R. Nilsson, S. Hornemann, G. Manco, M. Polymenidou, P. Schwarz, M. Leclerc, P. Hammarström, K. Wüthrich, A. Aguzzi, *Nat. Methods* 4 (2007) 1023–1030.
- [6] L.A. Munishkina, A.L. Fink, *Biochim. Biophys. Acta* 1768 (2007) 1862–1885.
- [7] M. Amaro, D.J.S. Birch, O.J. Rolinski, *Phys. Chem. Chem. Phys.* 13 (2011) 6434–6441.
- [8] M.J. Roberti, J. Fölling, M.S. Celej, M. Bossi, T.M. Jovin, E.A. Jares-Erijman, *Biophys. J.* 102 (2012) 1598–1607.
- [9] S.L. Shammass, G.A. Garcia, M. Kjaergaard, M.H. Horrocks, N. Shivji, E. Mandelkow, T.P.J. Knowles, E. Mandelkow, D. Klenerman, *Nat. Commun.* 6 (2015) 7025.
- [10] D. Pinotsi, G.S. Kaminski Schierle, C.F. Kaminski, *Methods Mol. Biol.* 1303 (2016) 125–141.
- [11] S.B. Padrick, A.D. Miranker, *J. Mol. Biol.* 308 (2001) 783–794.
- [12] N. Nespovityaya, J. Gath, K. Barylyuk, C. Seuring, B.H. Meier, R. Riek, *J. Am. Chem. Soc.* 138 (2016) 846–856.
- [13] E.S. Voropai, M.P. Samtsov, K.N. Kaplevskii, A.A. Maskevich, V.I. Stepuro, O.I. Povarov, I.M. Kuznetsova, K.K. Turoverov, A.L. Fink, V.N. Uverskii, *J. App. Spectrosc.* 70 (2003) 868–874.
- [14] N.P. Cook, K. Kilpatrick, L. Segatori, A.A. Martí, *J. Am. Chem. Soc.* 134 (2012) 20776–20782.
- [15] A. Aliyan, B. Kirby, C. Pennington, A.A. Martí, *J. Am. Chem. Soc.* 138 (2016) 8686–8689.
- [16] Y. Hong, L. Meng, S. Chen, C.W.T. Leung, L.-T. Da, M. Faisal, D.-A. Silva, J. Liu, J.W.Y. Lam, X. Huang, B.Z. Tang, *J. Am. Chem. Soc.* 134 (2012) 1680–1689.
- [17] N.D. Younan, J.H. Viles, *Biochemistry* 54 (2015) 4297–4306.
- [18] K.D. Volkova, V.B. Kovalska, A.O. Balanda, M.Y. Losytskyy, A.G. Golub, R.J. Vermeij, V. Subramaniam, O.I. Tolmachev, S.M. Yarmoluk, *Bioorg. Med. Chem.* 16 (2008) 1452–1459.
- [19] J. Thompson, T.W. Herling, M. Kubánková, A. Vyšniauskas, T.P.J. Knowles, M.K. Kuimova, *J. Phys. Chem. B* 119 (2015) 10170–10179.
- [20] J. Mohanty, S.D. Choudhury, H. Pal, A.C. Bhasikuttan, *Chem. Commun.* 48 (2012) 2403–2405.
- [21] M.K. Kuimova, *Phys. Chem. Chem. Phys.* 14 (2012) 12671–12686.
- [22] M.K. Kuimova, G. Yahioğlu, J.A. Levitt, K. Suhling, *J. Am. Chem. Soc.* 130 (2008) 6672–6673.
- [23] M.K. Kuimova, S.W. Botchway, A.W. Parker, M. Balaz, H.A. Collins, H.L. Anderson, K. Suhling, P.R. Ogilby, *Nat. Chem.* 1 (2009) 69–73.
- [24] M.A. Haidekker, E.A. Theodorakis, *Org. Biomol. Chem.* 5 (2007) 1669–1678.
- [25] M. B. Pepys, P. N. Hawkins, D. R. Booth, D. M. Vigushin, G. A. Tennent, A. K. Soutar, N. Totty, O. Nguyen, C. C. Blake, C. J. Terry, T. G. Feast, A. M. Zalin and J. J. Hsuan, *Nature* 362, 553–557.
- [26] D.R. Booth, M. Sunde, V. Bellotti, C.V. Robinson, W.L. Hutchinson, P.E. Fraser, P.N. Hawkins, C.M. Dobson, S.E. Radford, C.C.F. Blake, M.B. Pepys, *Nature* 385 (1997) 787–793.
- [27] D.E. Kuehner, J. Engmann, F. Fergg, M. Wernick, H.W. Blanch, J.M. Prausnitz, *J. Phys. Chem. B* 103 (1999) 1368–1374.
- [28] R. Wetzel, S.R. Halualani, J.T. Stults, C. Quan, *Bioconj. Chem.* 1 (1990) 114–122.
- [29] S. Mädl, C. Bich, D. Touboul, R. Zenobi, *J. Mass Spectrom.* 44 (2009) 694–706.
- [30] S. Kalkhof, A. Sinz, *Anal. Bioanal. Chem.* 392 (2008) 305–312.
- [31] M.A. Digman, V.R. Caiola, M. Zama, E. Gratton, *Biophys. J.* 94 (2008) L14–L16.
- [32] M.E. Sanborn, B.K. Connolly, K. Gurunathan, M. Levitus, *J. Phys. Chem. B* 111 (2007) 11064–11074.
- [33] E. Åkesson, V. Sundström, T. Gillbro, *Chem. Phys.* 106 (1986) 269–280.
- [34] A. Vyšniauskas, M. Qurashi, N. Gallop, M. Balaz, H.L. Anderson, M.K. Kuimova, *Chem. Sci.* 6 (2015) 5773–5778.
- [35] Y. Wu, M. Štefl, A. Olzyńska, M. Hof, G. Yahioğlu, P. Yip, D.R. Casey, O. Ces, J. Humpolíčková, M.K. Kuimova, *Phys. Chem. Chem. Phys.* 15 (2013) 14986–14993.
- [36] J.T. Mika, A.J. Thompson, J. Hofkens, M.K. Kuimova, *Biophys. J.* 108 (2015) 542a.
- [37] I. López-Duarte, T.T. Vu, M.A. Izquierdo, J.A. Bull, M.K. Kuimova, *Chem. Commun.* 50 (2014) 5282–5284.
- [38] P. Loison, N.A. Hosny, P. Gervais, D. Champion, M.K. Kuimova, J.M. Perrier-Cornet, *Biochim. Biophys. Acta* 1828 (2013) 2436–2443.
- [39] H. Zhu, J. Fan, M. Li, J. Cao, J. Wang, X. Peng, *Chemistry* 20 (2014) 4691–4696.
- [40] M.R. Dent, I. López-Duarte, C.J. Dickson, N.D. Geoghegan, J.M. Cooper, I.R. Gould, R. Krams, J.A. Bull, N.J. Brooks, M.K. Kuimova, *Phys. Chem. Chem. Phys.* 17 (2015) 18393–18402.
- [41] J.A. Levitt, M.K. Kuimova, G. Yahioğlu, P.-H. Chung, K. Suhling, D. Phillips, *J. Phys. Chem. C* 113 (2009) 11634–11642.
- [42] N.A. Hosny, G. Mohamedi, P. Rademeyer, J. Owen, Y. Wu, M.X. Tang, R.J. Eckersley, E. Stride, M.K. Kuimova, *Proc. Natl. Acad. Sci. U. S. A.* 110 (2013) 9225–9230.
- [43] M. Ahmed, J. Davis, D. Aucoin, T. Sato, S. Ahuja, S. Aimoto, J.I. Elliott, W.E. Van Nostrand, S.O. Smith, *Nat. Struct. Mol. Biol.* 17 (2010) 561–567.
- [44] L. Shimolina, M.A. Izquierdo, I. López-Duarte, J.A. Bull, M. Shirmanova, L. Klapshina, E. Zagaynova, M.K. Kuimova, *Sci. Rep.* 7 (2017) 41097.
- [45] Y.K. Al-Hilaly, T.L. Williams, M. Stewart-Parker, L. Ford, E. Skaria, M. Cole, W.G. Bucher, K.L. Morris, A.A. Sada, J.R. Thorpe, L.C. Serpell, *Acta Neuropathol. Commun.* 1 (2013) 83.
- [46] P.S. Vassar, C.F.A. Culling, *Arch. Pathol.* 64 (1959) 487–494.
- [47] M. Jungbauer, C. Yu, K.J. Laxton, M.J. LaDu, *J. Mol. Recognit.* 22 (2009) 403–413.
- [48] J. Násica-Labouze, P.H. Nguyen, F. Sterpone, O. Berthoumieu, N.-V. Buchete, S. Coté, A. De Simone, A.J. Doig, P. Faller, A. Garcia, A. Laio, M.S. Li, S. Melchionna, N. Mousseau, Y. Mu, A. Paravastu, S. Pasquali, D.J. Rosenman, B. Strodel, B. Tarus, J.H. Viles, T. Zhang, C. Wang, P. Derreumaux, *Chem. Rev.* 115 (2015) 3518–3563.
- [49] U. Das, G. Hariprasad, A.S. Ethayathulla, P. Manral, T.K. Das, S. Pasha, A. Mann, M. Ganguli, A.K. Verma, R. Bhat, S.K. Chandrayan, S. Ahmed, S. Sharma, P. Kaur, T.P. Singh, A. Srinivasan, *PLoS One* 2 (2007) e1176.
- [50] T. Tomiyama, A. Shoji, K. Kataoka, Y. Suwa, S. Asano, H. Kaneko, N. Endo, *J. Biol. Chem.* 271 (1996) 6839–6844.
- [51] Q. Wang, X. Yu, L. Li, J. Zheng, *Curr. Pharm. Des.* 20 (2014) 1223–1243.